IEEE Open Journal of
Antennas and Propagation

Received 4 July 2023; revised 3 August 2023; accepted 4 August 2023. Date of publication 10 August 2023; date of current version 25 August 2023.

Digital Object Identifier 10.1109/OJAP.2023.3303929

Coupled Array of Diverse Elements for Wideband High Spherical Coverage

QUANGANG CHEN [1] (Graduate Student Member, IEEE), VELI-PEKKA KUTINLAHTI [1], JAAKKO HAARLA [1,2], ANU LEHTOVUORI [1], AND VILLE VIIKARI [1] (Senior Member, IEEE)

[1]Department of Electronics and Nanoengineering, Aalto University School of Electrical Engineering, 00076 Espoo, Finland

[2]VTT Technical Research Centre of Finland, 02150 Espoo, Finland

CORRESPONDING AUTHOR: Q. CHEN (e-mail: quangang.chen@aalto.fi)

This work was supported by the Business Finland through the RF Sampo Project.

ABSTRACT We propose a flexible cluster array concept utilizing diverse antenna elements and the mutual coupling among them to improve the spherical coverage. This innovative approach can not only enhance the impedance matching but also improve the beamforming performance across a wide frequency band by adjusting excitation amplitudes and phases. Equations are derived to achieve specific objectives such as minimizing the total active reflection coefficient or maximizing the realized gain of an antenna array. To validate the concept, we employ a cluster array consisting of eight non-identical patch antenna elements with strong mutual coupling. When compared to a conventional four-element patch antenna array of the same size, the cluster array exhibits high beamforming capability over a wider frequency band. Simulated and measured results confirm that the operational frequency band can be extended from 24.5–26.5 GHz to 24.5–29.5 GHz, while maintaining a spherical coverage of over 6 dBi at the 50%-tile cumulative distribution function (CDF) of maximum realized gain.

INDEX TERMS Multiport antenna, mutual coupling, beamforming, reconfigurable antenna, CDF, mm-wave.

I. INTRODUCTION

IN THE era preceding 5G, a primary focus in mobile phone antenna design was on wideband impedance matching. Through innovative design techniques and the use of advanced materials, researchers and engineers strived to achieve optimal impedance matching across all operational bands for a stand-alone antenna, reducing signal reflection and maximizing power transfer [1], [2], [3], [4], [5], [6].

However, with the development of communication technologies the utilization of multi-port antenna systems has become crucial to improve their radiation capabilities. Accordingly, when forming an antenna array to maintain the wideband performance, mutual coupling among antenna elements can be a problem that needs to be addressed [7], [8], [9], [10]. In contrast, tightly coupled dipole arrays (TCDA) leverage strong mutual coupling to achieve broadband performance [11], [12], [13], [14]. Recently, a cluster concept has been reported in which frequency is reconfigured by adjusting the amplitudes and phases of excitation signals of coupled radiators [15]. The concept so far has been demonstrated for mobile devices operating in low frequency bands [16].

Millimeter-wave (mm-wave) technology is a key part of 5G and future 6G wireless networks, which allow higher data rates and more capacity. However, one of the major challenges of mm-wave technology is signal propagation. Consequently, beamforming capability is crucial for mm-wave antennas and networks allowing for the efficient and targeted transmission of wireless signals. In order to evaluate the performance of beam-steerable transceivers in user equipment (UE) at mm-wave frequencies, 3GPP has introduced a standard based on the cumulative distribution function (CDF) of the equivalent isotropic radiated power (EIRP) [17]. Recently, this standard has drawn increasing interest in antenna designs that aim to maximize the CDF of EIRP. The influence of different array locations in a smartphone was

analyzed to realize better spherical coverage [18], [19], [20]. All studies were conducted specifically at the frequency of 28 GHz because of the narrowband antennas. As one of the designated mm-wave frequency bands spans from 24.25-29.5 GHz, it is imperative for antennas to exhibit excellent beamforming capabilities across this broad frequency range. However, achieving this objective poses a challenge due to the limited available volume for antennas within mobile devices [21].

The novelty of this work lies in applying the cluster concept to the mm-wave frequency band, where beamforming capability is crucial for mobile communications, as derived equations for the maximum realized gain in Section II-B are utilized. While previous cluster studies have primarily focused on impedance matching reconfiguration, the objective for mm-wave antennas is to enhance the beamforming capability across a wide frequency band. For the first time, we present a novel cluster array that combines the previously presented cluster concept with conventional arrays. This cluster array consists of eight coupled elements with the same polarization to enable beam steering capability. However, these eight coupled elements differ in length, allowing for reconfigurability through the adjustment of feeding weights. We simulate, analyze, and compare the performance of the cluster array with a traditional four-element patch antenna array of the same size. Furthermore, we fabricate prototypes and conduct measurements to validate the advantages of our proposed approach.

II. THEORY

Low-frequency mobile communications (e.g., <2 GHz) exhibit longer wavelengths compared to the size of mobile devices, resulting in an omnidirectional radiation pattern. The main challenge lies in achieving wideband impedance matching. However, in the mm-wave frequency band, the allocation of feeding weights is vital to enable beam steering using directive antenna elements. Consequently, new formulas have been derived to optimize the performance of beamforming for the cluster concept in the mm-wave frequency band.

In the following, We sequentially demonstrate the selection of excitation weights for optimal active impedance matching and maximum realized gain of an array.

A. SELECTING WEIGHTS FOR THE BEST ACTIVE MATCHING

The reflections occurring at the interface between an antenna array and a multi-channel RFIC (see Fig. 1) can be characterized as

$$\boldsymbol{b} = \boldsymbol{S}\boldsymbol{a} \tag{1}$$

where $\boldsymbol{a}$ collects incoming voltage waves in a vector, $\boldsymbol{b}$ represents the reflected wave vector, and $\boldsymbol{S}$ denotes the scattering matrix of the multiport antenna system. It is important to note that $\boldsymbol{b}$ is influenced not only by the reflection coefficient but also by the transmission coefficient when all ports are actively excited simultaneously. Therefore, all the entries

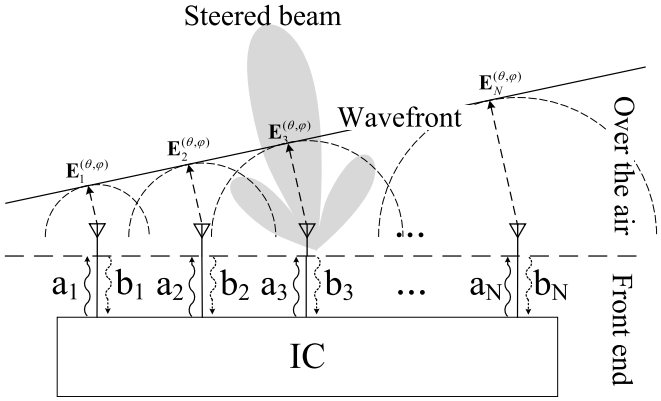

FIGURE 1. Overall picture of antenna array system.

included in the scattering matrix can be used to minimize the reflected wave by appropriately selecting the excitation vector $\boldsymbol{a}$.

In the case of a multi-port antenna array, the total active reflection coefficient (TARC) offers a comprehensive assessment of the overall impedance matching, in contrast to considering only the reflection coefficient of a single port [22]. TARC is defined as the square root of the ratio between the reflected power and incident power

$$\text{TARC} = \sqrt{\frac{\boldsymbol{b}^H\boldsymbol{b}}{\boldsymbol{a}^H\boldsymbol{a}}} = \sqrt{\frac{\boldsymbol{a}^H\boldsymbol{S}^H\boldsymbol{S}\boldsymbol{a}}{\boldsymbol{a}^H\boldsymbol{a}}}. \tag{2}$$

In the calculation of the TARC, the radicand represents a Rayleigh quotient, which is minimized when the vector $\boldsymbol{a}$ corresponds to the eigenvector of the matrix product $\boldsymbol{S}^H\boldsymbol{S}$ associated with the smallest eigenvalue. To accommodate the frequency dependence of the S-parameters, frequency-specific feed weights are utilized to realize frequency reconfigurability. Similar approach has been used in [15], [16], [23].

B. SELECTING WEIGHTS FOR THE HIGHEST GAIN

Next, the objective is to maximize the array gain at one angle and frequency. It is well-known that

$$P_{\text{rad}} = \oint_{\Omega} U d\Omega = \int_0^{2\pi}\int_0^{\pi} U \sin\theta d\theta d\varphi \tag{3}$$

where P_{rad} represents the total radiation power and U is the radiation intensity [24]. When using beam-forming technology, the radiation intensity of each solid angle is more meaningful and it can be written as

$$U_{(\theta,\varphi)} = \frac{1}{2\eta}\left(|E_{\theta(\theta,\varphi)}|^2 + |E_{\varphi(\theta,\varphi)}|^2\right) \tag{4}$$

where η represents the wave impedance of free space, and E_θ and E_φ are the orthogonally polarized components of the electric field in the far field. In the case of an N-port antenna system, as illustrated in Fig. 1, the total radiated field is the cumulative effect of the fields generated by each individual element. Consequently, the total radiated field, $\boldsymbol{E}_{\text{total}}$, for a

specific steered beam, is a vector combination of the fields emitted by all radiators:

$$\boldsymbol{E}_{\text{total}} = \boldsymbol{E}_1 + \boldsymbol{E}_2 + \cdots + \boldsymbol{E}_N. \tag{5}$$

This can be expressed by two orthogonal vectors as follows:

$$\begin{aligned} E_{\theta,total} &= E_{\theta,1} + E_{\theta,2} + \cdots + E_{\theta,N} \\ E_{\varphi,total} &= E_{\varphi,1} + E_{\varphi,2} + \cdots + E_{\varphi,N}. \end{aligned} \tag{6}$$

The realized gain can be presented as

$$G^r_{(\theta,\varphi)} = \frac{4\pi\, U_{(\theta,\varphi)}}{P_{\text{inc}}}. \tag{7}$$

Here, the transmission coefficient $\boldsymbol{T}_{(\boldsymbol{\theta},\boldsymbol{\varphi})}$ over the air is defined as the ratio of the E-field vector to the incident wave vector:

$$\boldsymbol{E}_{(\theta,\varphi)} = \boldsymbol{T}_{(\theta,\varphi)}\boldsymbol{a}_{(\theta,\varphi)}. \tag{8}$$

Combining (4), (6), (7), and (8), produces the following formulation for realized gain

$$G^r = \frac{4\pi}{\eta}\frac{\boldsymbol{a}^H\boldsymbol{T}^H\boldsymbol{T}\boldsymbol{a}}{\boldsymbol{a}^H\boldsymbol{a}}. \tag{9}$$

The obtained Rayleigh quotient is maximized when the feeding vector $\boldsymbol{a}$ is the eigenvector of $\boldsymbol{T}^H\boldsymbol{T}$ corresponding to the largest eigenvalue. Therefore, the maximum array gain at different angles and frequencies can be obtained by adjusting the excitation vector.

In mobile devices with limited internal space, antenna arrays face challenges in attaining both high gain and wide bandwidth due to the significant mutual coupling between antenna elements. However, we have changed the design paradigm so that instead of designing independent, isolated elements, we design a cluster of multiple antennas as a unified entity. Our previous research has demonstrated that mutual coupling among antennas can be leveraged to reduce the TARC of a multi-port antenna system, thereby improving the total efficiency. Next, we will illustrate how the cluster concept improve not only the impedance matching but also the spherical coverage across a wide band despite the high mutual coupling.

III. ANTENNA SIMULATION AND CALCULATION

In this section, we implement the proposed cluster array concept by simulating basic patch antennas in CST. Subsequently, we analyze the obtained simulation results using MATLAB. By utilizing the derived equations presented in Section II, we are able to obtain the minimum TARCs or maximum realized gains, and determine the required feeding weights for the two distinct targets. Our main objective is to demonstrate the enhanced spherical coverage provided by the cluster array concept when compared to conventional antenna arrays. Consequently, we did not extensively optimize the antenna structures or compare variations in dimensions. Patch antennas are chosen for this purpose, and they are also easy to produce.

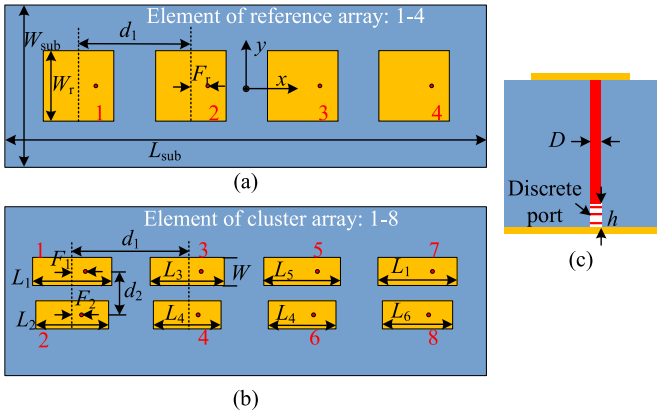

FIGURE 2. (a) Top view of the reference patch antenna layer. (b) Top view of the proposed cluster layer. (c) Cross section of the antenna structure.

TABLE 1. Specific dimensions of the antenna structures.

Parameters	W_{sub}	L_{sub}	d_1	d_2	W	F_1
Values(mm)	5.5	24	5.5	1.7	1	0.45
Parameters	F_2	L_1	L_2	L_3	L_4	L_5
Values(mm)	0.3	3.1	2.85	2.9	2.65	3
Parameters	L_6	W_r	F_r	D	h	
Values(mm)	2.75	2.9	0.55	0.15	0.1	

A. ANTENNA CONFIGURATION

Figure 2(a) illustrates an eight-element patch antenna cluster constructed on the top surface of a Rogers-4003 substrate (ϵ_r=3.5 and tanδ=0.002) with a thickness of 0.508 mm. The resonance of the patch antenna is primarily influenced by the length of the side within the E-plane. By optimizing the different patch lengths (L_i), various resonances are distributed across the desired frequency band, and one more resonances is excited at the edge frequencies (24.5 and 29.5 GHz), respectively, to enhance the performance throughout the frequency band of interest. In addition, the length of the side within the H-plane is compressed to accommodate all the elements within a limited area. Probes connecting with 50-Ω discrete ports are employed for feeding these elements during simulations as shown in Fig. 2 (c).

For comparative purposes, a conventional four-element square patch antenna array, shown in Fig. 2 (b), is also fabricated. This reference patch array employs the same substrate and feeding structures as the cluster array. It is noteworthy that the eight-element cluster array and the four-element reference array occupy a nearly equivalent area. Specific dimensions are provided in Table 1.

B. IMPEDANCE MATCHING

Figure 3 (a) presents the simulated passive reflection coefficients of the cluster array, along with the minimum TARC values. Despite the relatively high mutual coupling of −5 dB observed in the cluster array (as depicted in Fig. 3 (b)), effective impedance matching is attained through the utilization of optimal feeding weights for the eight

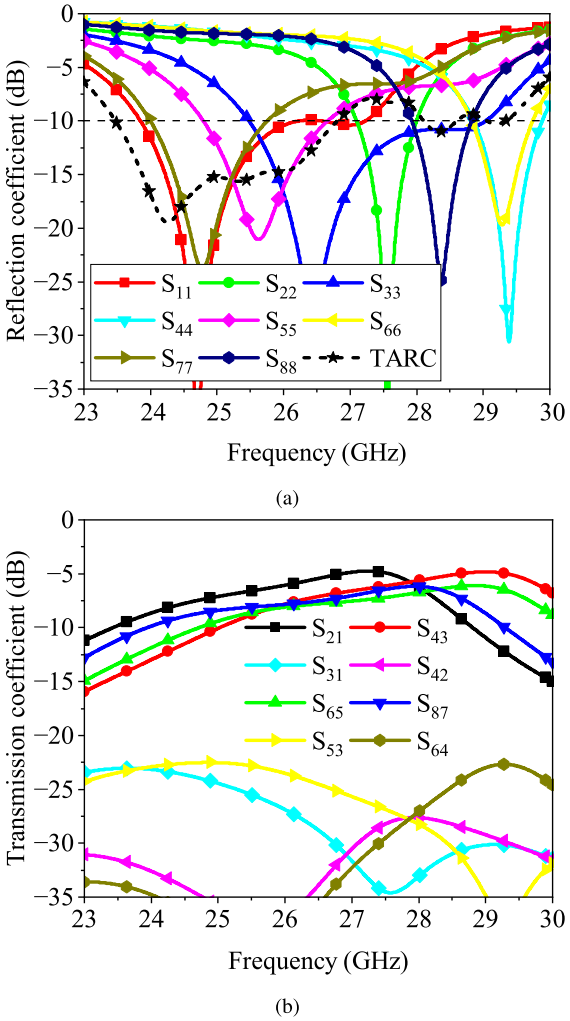

FIGURE 3. Simulated scattering parameters of the cluster array. (a) Reflection coefficients of each antenna port and the minimum TARC with optimal feeding weights. (b) Transmission coefficients.

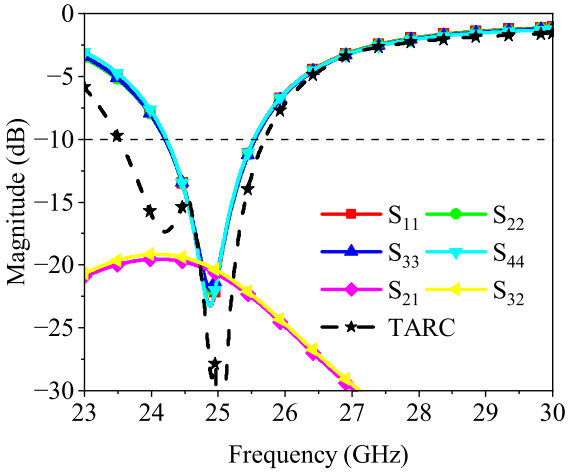

FIGURE 4. S-parameters and TARCs with optimized feed weights of the reference array.

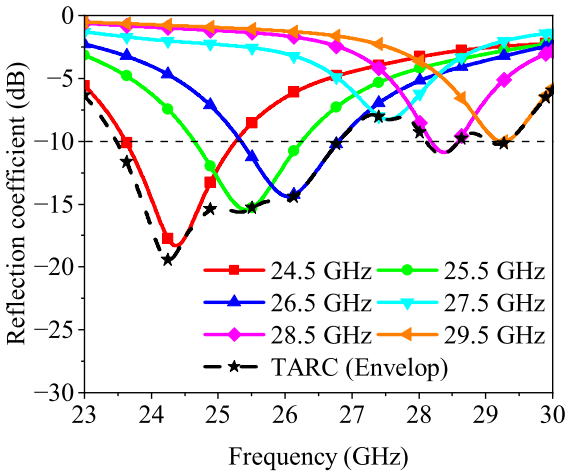

FIGURE 5. TARCs of the cluster array with specific excitation vectors corresponding to different frequencies, and the minimum TARC (Envelope) corresponding to all frequencies.

ports. The bandwidth of the cluster array exhibits a much wider range in terms of TARC compared to the reference arrays as shown in Fig. 4. This enhancement is attributed to the presence of different resonances distributed across the operational frequency band, as reported in our previous studies [23].

Figure 5 illustrates specific examples of achieving the frequency band ranging from 24.5 to 29.5 GHz. Instantaneous bandwidths exceeding 400 MHz can be covered with optimal feeding weights that enable reaching the minimum TARC at the corresponding center frequency. The envelope curve in the figure represents the minimum TARCs across all frequencies. Furthermore, Table 2 lists the necessary feeding weights for attaining the minimum TARCs at selected frequencies. It also provides information on the peak realized gain and the directions of the main lobes corresponding to the three working status of the cluster.

C. SPHERICAL COVERAGE GAIN

The realized gain of an antenna array, which considers practical factors such as impedance matching on the board and radiation properties in the air, provides an effective means to assess array performance. The maximum realized gain at a specific angle and frequency can be calculated by synthesizing the port-specific radiation patterns using (9). When considering the characteristics of mobile devices, spherical coverage becomes more meaningful. According to the 3GPP standard, CDF curves of the maximum realized gain are utilized to evaluate the spherical coverage performance for mobile devices. The mathematical definition of CDF is given by

$$F(G^r) = P\left(G^r_{(\theta,\varphi)} <= G^r\right) \tag{10}$$

where the right-hand side means the probability that the value of $G^r_{(\theta,\varphi)}$ is less than or equal to a threshold value G^r. Due to the directive radiation pattern of patch antennas,

TABLE 2. Optimal excitation vectors of the cluster array for the minimum TARCs at different frequencies and corresponding beams.

port	24.5 GHz	26.5 GHz	29.5 GHz
1	$0.58\angle 139.9$	$0.10\angle -43.5$	$0.03\angle -11.4$
2	$0.26\angle -165.0$	$0.03\angle -5.0$	$0.04\angle -88.1$
3	$0.19\angle -7.3$	$0.89\angle -26.9$	$0.30\angle 91.0$
4	$0.09\angle -23.7$	$0.40\angle -52.9$	$0.41\angle -60.1$
5	$0.32\angle 173.9$	$0.12\angle -137.0$	$0.34\angle -91.9$
6	$0.13\angle 156.6$	$0.08\angle -166.4$	$0.76\angle 127.7$
7	$0.61\angle 14.8$	$0.10\angle 37.2$	$0.01\angle 121.3$
8	$0.24\angle 0$	$0.05\angle 0$	$0.22\angle 0$
Gain$^{\#}$	6.3 dBi	5.8 dBi	5.7 dBi
Angle*	$\theta = 19°$ $\varphi = -6°$	$\theta = 44°$ $\varphi = -4°$	$\theta = 54°$ $\varphi = -20°$

$^{\#}$: corresponding maximum realized gains.

* : directions of the corresponding maximum realized gain.

the calculation of spherical coverage takes into account the upper hemisphere ($+z$).

Figure 6 (a) illustrates the CDF curves of the maximum realized gains for the cluster array and the reference array at different frequencies. The excitation vectors for both arrays are calculated based on (9). It is worth noting that the total feeding power of all ports has been normalized to 1 W. Upon observation, it is evident that both the reference array and the cluster array demonstrate satisfactory performance at 24.5 GHz, 25.5 GHz, and 26.5 GHz. However, as the frequency increases further, the performance of the reference array begins to deteriorate, while the cluster array still maintains consistent spherical coverage across the entire frequency band. Notably, at 29.5 GHz, the cluster array exhibits a spherical coverage gain that is 5 dBi higher than that of the reference array at the 50 %-tile CDF.

In order to obtain a comprehensive understanding of the improvement in realized gain, Fig. 6 (b) presents the CDF curves of the corresponding gains for the cluster array and the reference array. These gains are calculated by removing the impact of impedance mismatch from the maximum realized gains used in Fig. 6 (a). It can be observed that the proposed cluster array still achieves an approximately 1.5-dB improvement at the 50 %-tile CDF compared to the reference array. In other words, the proposed cluster array enhances the realized gain primarily by achieving impedance matching and partly through gain improvement in a wide band, while maintaining the same physical size as the reference array.

Sufficient bandwidth should be covered, e.g., larger than 400 MHz for practical applications. As shown in Fig. 5, we have demonstrate the bandwidth when the purpose is to achieve the minimum TARC. Here, Fig. 7 is plotted to illustrate the instantaneous bandwidth when the objective is to improve spherical coverage. Both the cluster array and

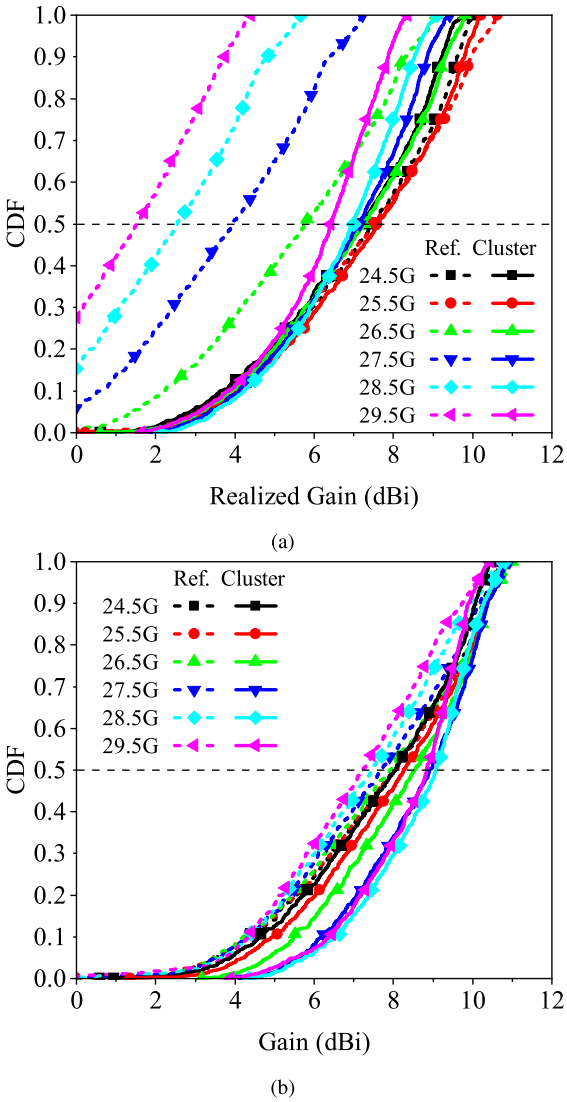

FIGURE 6. Spherical coverage performance for the cluster array and reference array at different frequencies characterized by (a) CDF curves of the maximum realized gains. (b) CDF curves of the corresponding gains.

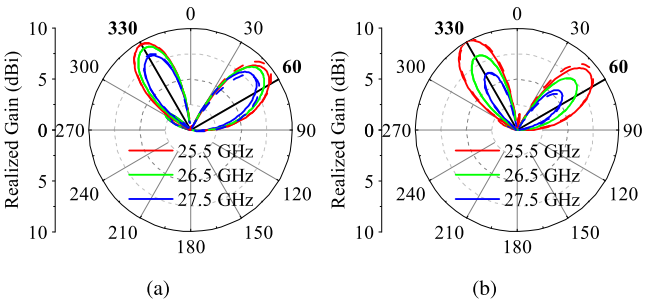

FIGURE 7. Simulated beams of (a) the cluster array and (b) the reference array towards $\theta = 60°$ or $\theta = -30°$ in $\varphi = 0°$. The feeding weights of these beams are selected only at 26.5 GHz (solid line) or corresponding frequencies (dashed line).

reference array of antennas are fed with their respective calculated feeding weights. For the solid lines, the beams are generated with excitation vectors which can maximize

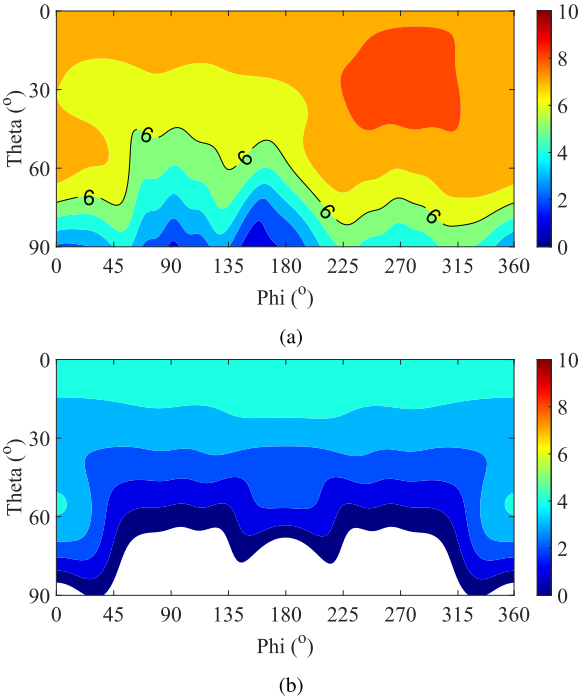

FIGURE 8. Simulated total scan patterns of the maximum realized gain at 29.5 GHz with optimal feeding weights for (a) the cluster array. (b) the reference array.

the realized gain towards $\theta = 60°$ or $\theta = -30°$ in $\varphi = 0°$ cut at 26.5 GHz. It can be seen that using the same excitation vectors, the beams at different frequencies still point to the desired directions, although the employed feeding weights are not the optimal ones for the steered beams at 25.5 and 27.5 GHz. The dashed lines show the results with optimal excitations for each corresponding frequency. Comparing the solid lines and dashed lines in the same color and direction, small improvements can be found at 25.5 and 27.5 GHz in Fig. 7 (a) due to the optimal feeding weights. Moreover, it is worth noting that the reference array exhibits a significant difference in realized gain between different frequencies as shown in Fig. 7 (b), despite the beams pointing in the same direction. Therefore, we can conclude that the cluster concept can still support sufficient bandwidth even when the objective is the improvement in spherical coverage.

To intuitively demonstrate the beamforming capability, Fig. 8 presents the 2D total scan patterns at 29.5 GHz, which depict the maximum realized gains with optimized feed coefficients towards all angles in the upper hemisphere (+z). The scan patterns highlight the significant improvement of the cluster array over the reference array, as the realized gains of the proposed cluster array are mostly above 6 dBi, while the realized gains at all angles of the reference array remain below 4 dBi.

IV. EXPERIMENTS

Fig. 9 displays the feeding lines and the fabricated prototypes of the reference array and the cluster array. An additional layer is added underneath the ground plane to incorporate the

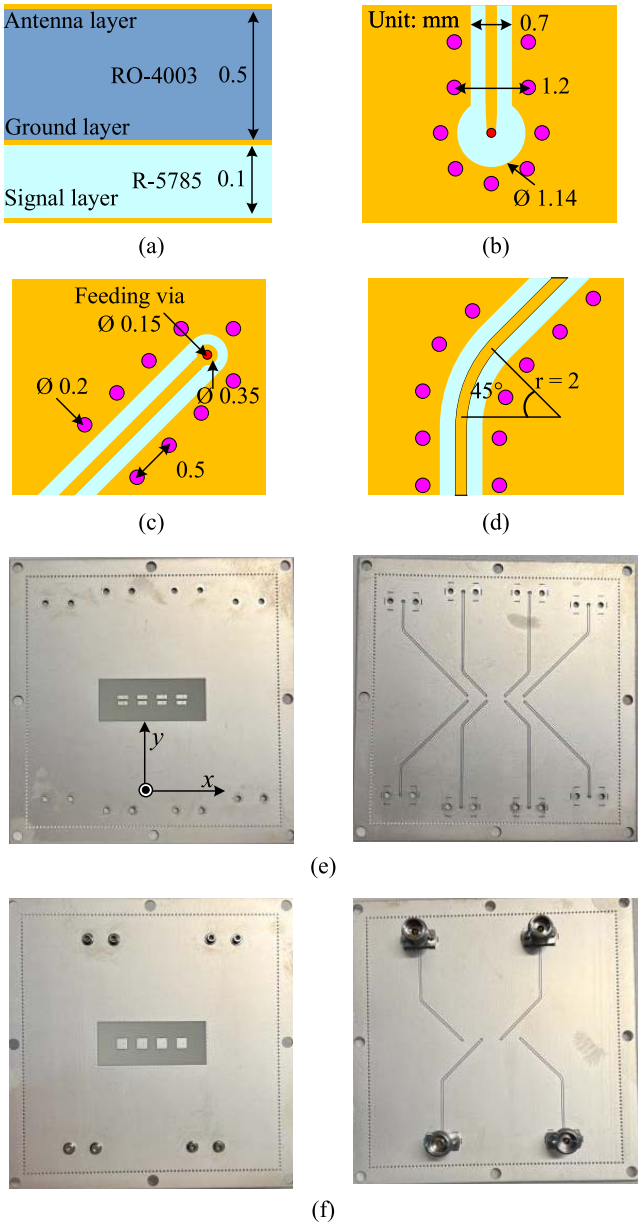

FIGURE 9. (a) Cross section of the stack-up. Details of the feeding network for (b) vertical launch connectors and (c) feeding probes (d) bend in the feeding lines. Fabricated prototypes of (e) the cluster array and (f) the reference array.

feeding network as shown in Fig. 9 (a). The prepreg material is R-5680 with $\varepsilon_r = 3.55$ and $\tan\delta = 0.004$. The details of feeding lines are illustrated in Fig. 9 (b), (c), and (d). All the microstrip feeding lines on the bottom layer have a width of 0.19 mm and a length of 33 mm. In addition, the top layer is covered with metal to suppress surface waves, leaving a 12×30 mm^2 window for radiation. For practicality and ease of measurement, the dimensions W_{sub} and L_{sub} are enlarged to 60 mm to accommodate eight vertical launch connectors, while the other dimensions remain the same as stated in Table 1. Reflection coefficients of the simulated and fabricated prototypes are shown in Fig. 10. Since the main object of this work is to show the improvement in

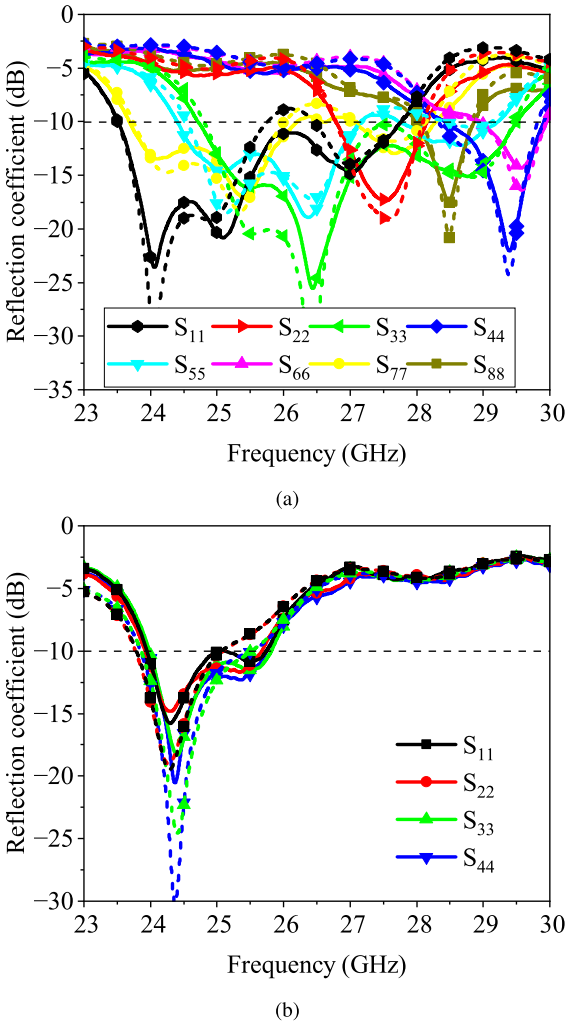

FIGURE 10. Measured (solid lines) and simulated (dashed lines) reflection coefficients for the (a) cluster array and (b) reference array.

spherical coverage, the calculation of TARCs for the fabricated prototypes is not performed in this section, and only reflection coefficients are demonstrated for brevity.

The far-field results are first measured in an anechoic chamber by feeding one port at a time and terminating unused ports to 50-Ω loads. The maximum realized gains towards different steering angles at different frequencies are then calculated in MATLAB using (9) for the cluster array and reference array. CDF curves of the maximum realized gains for both arrays are depicted in Fig. 11. It can be noted that the spherical coverage gain of the reference array is higher than 5.5 dBi from 24.5 GHz to 26.5 GHz at the 50%-tile CDF, but it gradually drops to 2 dBi as the frequency increases to 29.5 GHz. In contrast, the proposed cluster array demonstrates the ability to maintain a high level of spherical coverage gain (>6 dBi at the 50%-tile CDF) over the desired frequency band from 24.5 to 29.5 GHz. These measurement results support the notion that spherical coverage can be maintained at a high level throughout the frequency band of interest, effectively increasing the bandwidth characterized by spherical coverage.

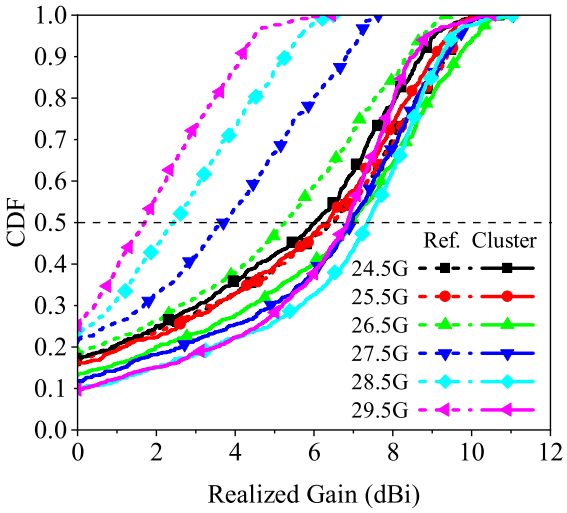

FIGURE 11. Measured spherical coverage gain CDF curves of the cluster and reference array at different frequencies.

TABLE 3. Optimal excitation vectors of the cluster array for achieving maximum realized gain of the cluster array towards different θ angles in $\varphi = 0°$ cut at 29.5 GHz.

port	$\theta = -60°$	$\theta = -30°$	$\theta = 0°$
1	$0.43\angle -74.5$	$0.19\angle 119.2$	$0.25\angle 17.8$
2	$0.41\angle -86.6$	$0.24\angle 101.1$	$0.30\angle 15.5$
3	$0.53\angle 15.0$	$0.35\angle 125.3$	$0.35\angle -31.9$
4	$0.17\angle -72.5$	$0.34\angle 54.4$	$0.47\angle -108.5$
5	$0.37\angle -164.8$	$0.45\angle -135.6$	$0.38\angle -27.3$
6	$0.26\angle 74.7$	$0.45\angle 142.9$	$0.52\angle -105.6$
7	$0.21\angle 87.7$	$0.30\angle 63.2$	$0.12\angle 69.4$
8	$0.31\angle 0$	$0.42\angle 0$	$0.29\angle 0$

TABLE 4. Comparison between proposed design and references.

Ref.	Antenna type	Element number	Size (λ_0^2)	BW (GHz)	Adaptability
[6]	Patch	1×16	0.32×9.2	24.4–31.3	NO
[9]	Patch	1×4	0.46×1.51	33.2–37.2	NO
[10]	Patch	2×4	1.37×1.8	23.5–28	NO
[12]	TCDA	1×8	3.87×1.1	22.5–32.5	NO
This work	**Patch**	**2×4**	**0.24×1.75**	**24.5–29.5**	**YES**

Adaptability: the capacity of the proposed approach to smoothly adapt various antenna types.

Figure 12 illustrates the radiation pattern towards different steering angles for the reference and cluster arrays. The beams produce maximum realized gains in the directions $\theta = -60°: 30°: 60°$, $\varphi = 0°$ at 24.5 GHz and 29.5 GHz. These results confirm that the reference array and the cluster array have similar beam patterns at the same tilted angle at 24.5 GHz. However, the realized gain levels of the proposed cluster array are about 4.5 dB higher on average compared to those of the reference array at 29.5 GHz. In addition, Table 3

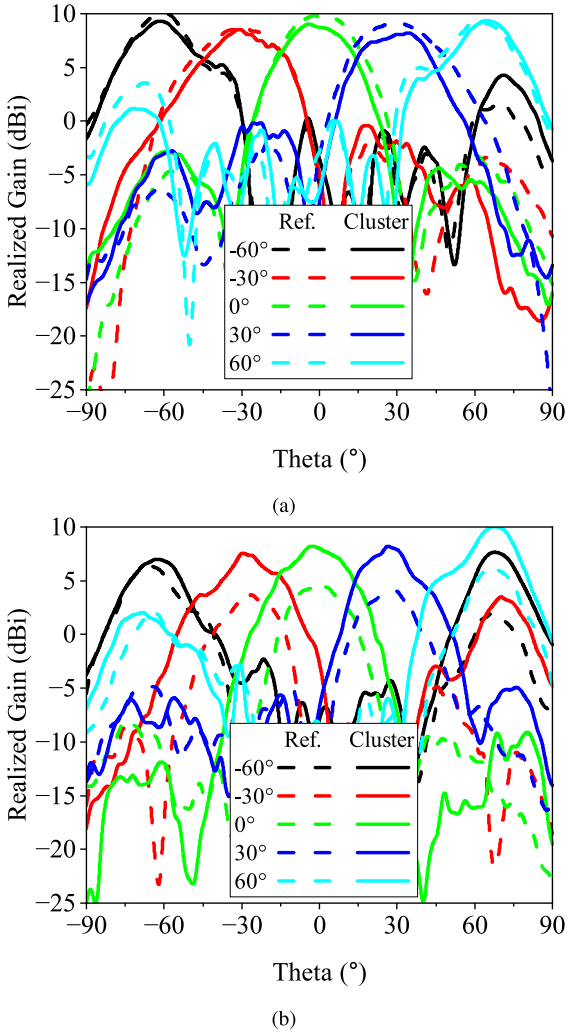

FIGURE 12. Measured beam scanning radiation patterns with specific feeding weights for the maximum realized gain of different angles in $\varphi = 0°$ cut at (a) 24.5 GHz. (b) 29.5 GHz.

demonstrates the corresponding optimal feeding weights for achieving maximum array gain towards different θ angles in $\varphi = 0°$ cut at 29.5 GHz.

Table 4 summarizes recent publications concerning wide operating frequency band. In [6], [9], and [10], the mutual coupling between the elements is minimized to avoid deterioration on the array's performance, while [12] and this work can achieve effective beamforming capability despite the high mutual coupling. Importantly, the proposed cluster array concept is not limited to specific antenna types or structures; it can be applied to various multi-port antenna designs.

V. CONCLUSION

This paper expands the cluster array concept to the mm-wave frequency band, where beamforming capability is crucial. By leveraging non-identical antenna elements, the cluster array maximizes the realized gain across a wide frequency band through the adjustment of feeding weights despite high mutual coupling between the elements. An eight-element cluster array demonstrates a 5-dB improvement of the spherical coverage at the 50%-tile CDF of realized gain at 29.5 GHz while maintaining the same level at 24.5 GHz, in comparison to a typical patch antenna array occupying the same area. From the perspective of spherical coverage, the bandwidth can be extended from 2 GHz (24.5–26.5 GHz) to 5 GHz (24.5–29.5 GHz). The cluster array concept offers a flexible approach to improve the spherical coverage performance for mobile devices of limited inner space. In this proof-of-concept study, simple antenna elements are utilized and the center-to-center distances of antenna elements in the E-plane are kept equal to eliminate their influence on beam steering. Future work will focus on the practical active antenna system such as integration with IC chips.

REFERENCES

[1] C.-L. Mak, K. Luk, K. Lee, and Y. Chow, "Experimental study of a microstrip patch antenna with an L-shaped probe," *IEEE Trans. Antennas Propag.*, vol. 48, no. 5, pp. 777–783, May 2000.

[2] E. Lee, P. Hall, and P. Gardner, "Compact wideband planar monopole antenna," *Electron. Lett.*, vol. 35, no. 25, pp. 2157–2158, 1999.

[3] Z. Ying, "Antennas in cellular phones for mobile communications," *Proc. IEEE*, vol. 100, no. 7, pp. 2286–2296, Jul. 2012.

[4] Z. N. Chen, T. S. P. See, and X. Qing, "Small printed ultrawideband antenna with reduced ground plane effect," *IEEE Trans. Antennas Propag.*, vol. 55, no. 2, pp. 383–388, Feb. 2007.

[5] P. Sohrabi, P. Rezaei, S. Kiani, and M. Fakhr, "A symmetrical SIW-based leaky-wave antenna with continuous beam scanning from backward-to-forward through broadside," *Wireless Netw.*, vol. 27, pp. 5417–5424, Sep. 2021.

[6] M. Khalily, R. Tafazolli, P. Xiao, and A. A. Kishk, "Broadband mm-Wave microstrip array antenna with improved radiation characteristics for different 5G applications," *IEEE Trans. Antennas Propag.*, vol. 66, no. 9, pp. 4641–4647, Sep. 2018.

[7] X.-T. Yuan, W. He, K.-D. Hong, C.-Z. Han, Z. Chen, and T. Yuan, "Ultra-wideband MIMO antenna system with high element-isolation for 5G smartphone application," *IEEE Access*, vol. 8, pp. 56281–56289, 2020.

[8] D. Gao, Z.-X. Cao, S.-D. Fu, X. Quan, and P. Chen, "A novel slot-array defected ground structure for decoupling microstrip antenna array," *IEEE Trans. Antennas Propag.*, vol. 68, no. 10, pp. 7027–7038, Oct. 2020.

[9] Z. Mousavi and P. Rezaei, "Millimetre-wave beam-steering array antenna by emphasising on improvement of butler matrix features," *IET Microw., Antennas Propag.*, vol. 13, no. 9, pp. 1287–1292, 2019.

[10] Y. Luo et al., "A zero-mode induced mmWave patch antenna with low-profile, wide-bandwidth and large-angle scanning for 5G mobile terminals," *IEEE Access*, vol. 7, pp. 177607–177615, 2019.

[11] B. Munk et al., "A low-profile broadband phased array antenna," in *IEEE Antennas Propag. Soc. Int. Symp., Dig., USNC/CNC/URSI North Amer. Radio Sci. Meeting*, vol. 2. Columbus, OH, USA, 2003, pp. 448–451.

[12] J.-Y. Shim, J.-G. Go, and J.-Y. Chung, "A 1-D tightly coupled dipole array for broadband mmWave communication," *IEEE Access*, vol. 7, pp. 8258–8265, 2019.

[13] J. P. Doane, K. Sertel, and J. L. Volakis, "A wideband, wide scanning tightly coupled dipole array with integrated balun (TCDA-IB)," *IEEE Trans. Antennas Propag.*, vol. 61, no. 9, pp. 4538–4548, Sep. 2013.

[14] J. Wang, X. Zhao, Y. Ye, and S. Liu, "A millimeter-wave ultrawideband tightly coupled dipole array antenna for vehicle communication," *IEEE Antennas Wireless Propag. Lett.*, vol. 21, no. 10, pp. 2135–2139, Oct. 2022.

[15] J.-M. Hannula, J. Holopainen, and V. Viikari, "Concept for frequency-reconfigurable antenna based on distributed transceivers," *IEEE Antennas Wireless Propag. Lett.*, vol. 16, pp. 764–767, 2017.
[16] R. Luomaniemi, J.-M. Hannula, R. Kormilainen, A. Lehtovuori, and V. Viikari, "Unbroken metal rim MIMO antenna utilizing antenna clusters," *IEEE Antennas Wireless Propag. Lett.*, vol. 18, no. 6, pp. 1071–1075, Jun. 2019.
[17] *User Equipment (UE) Radio Transmission and Reception; Part 2: Range 2 Standalone (Release 16)*, 3GPP Standard TS 38.101-2, Version 16.4.0, 2020.
[18] A. Hazmi et al., "Spherical coverage characterization of millimeter wave antenna arrays in 5G mobile terminals," in *Proc. 13th Eur. Conf. Antennas Propag. (EuCAP)*, Kraków, Poland, 2019, pp. 1–5.
[19] K. Zhao et al., "Spherical coverage characterization of 5G millimeter wave user equipment with 3GPP specifications," *IEEE Access*, vol. 7, pp. 4442–4452, Dec. 2018.
[20] T. Hahn and D. Manteuffel, "Millimeter wave user equipment beamforming concept compliant with 3GPP specifications," in *Proc. 17th Eur. Conf. Antennas Propag. (EuCAP)*, Florence, Italy, 2023, pp. 1–4.
[21] W. Hong, K.-H. Baek, and S. Ko, "Millimeter-wave 5G antennas for smartphones: Overview and experimental demonstration," *IEEE Trans. Antennas Propag.*, vol. 65, no. 12, pp. 6250–6261, Dec. 2017.
[22] M. Manteghi and Y. Rahmat-Samii, "Multiport characteristics of a wide-band cavity backed annular patch antenna for multipolarization operations," *IEEE Trans. Antennas Propag.*, vol. 53, no. 1, pp. 466–474, Jan. 2005.
[23] J.-M. Hannula, T. Saarinen, J. Holopainen, and V. Viikari, "Frequency reconfigurable multiband handset antenna based on a multichannel transceiver," *IEEE Trans. Antennas Propag.*, vol. 65, no. 9, pp. 4452–4460, Sep. 2017.
[24] C. A. Balanis, *Antenna Theory: Analysis and Design*. Hoboken, NJ, Wiley, 2005.